JOURNAL OF VIROLOGY, Nov. 2007, p. 12485–12495 Vol. 81, No. 22
0022-538X/07/$08.00+0 doi:10.1128/JVI.00972-07
Copyright © 2007, American Society for Microbiology. All Rights Reserved.

Human Rhinovirus Type 14 Gain-of-Function Mutants for oriI Utilization Define Residues of 3C(D) and 3Dpol That Contribute to Assembly and Stability of the Picornavirus VPg Uridylylation Complex▽

Miaoqing Shen,[1]† Qixin Wang,[1] Yan Yang,[2]‡ Harsh B. Pathak,[1]§ Jamie J. Arnold,[1] Christian Castro,[1] Stanley M. Lemon,[2] and Craig E. Cameron[1]*

Department of Biochemistry and Molecular Biology, Pennsylvania State University, University Park, Pennsylvania 16802,[1] and Institute for Human Infections and Immunity and Department of Microbiology and Immunology, University of Texas Medical Branch, Galveston, Texas 77555-1073[2]

Received 5 May 2007/Accepted 30 August 2007

VPg linkage to the 5′ ends of picornavirus RNAs requires production of VPg-pUpU. VPg-pUpU is templated by an RNA stem-loop (the cre or oriI) found at different locations in picornavirus genomes. At least one adaptive mutation is required for human rhinovirus type 14 (HRV-14) to use poliovirus type 3 (PV-3) or PV-1 oriI efficiently. One mutation changes Leu-94 of 3C to Pro; the other changes Asp-406 of 3Dpol to Asn. By using an in vitro VPg uridylylation system for HRV-14 that recapitulates biological phenotypes, we show that the 3C adaptive mutation functions at the level of 3C(D) and the 3D adaptive mutation functions at the level of 3Dpol. Pro-94 3C(D) has an expanded specificity and enhanced stability relative to wild-type 3C(D) that leads to production of more processive uridylylation complexes. PV-1/HRV-14 oriI chimeras reveal sequence specificity in 3C(D) recognition of oriI that resides in the upper stem. Asn-406 3Dpol is as active as wild-type 3Dpol in RNA-primed reactions but exhibits greater VPg uridylylation activity due to more efficient recruitment to and retention in the VPg uridylylation complex. Asn-406 3Dpol from PV-1 exhibits identical behavior. These studies suggest a two-step binding mechanism in the assembly of the 3C(D)-oriI complex that leads to unwinding of at least the upper stem of oriI and provide additional support for a direct interaction between the back of the thumb of 3Dpol and 3C that is required for 3Dpol recruitment to and retention in the uridylylation complex.

A peptide encoded by the 3B region of the picornavirus genome termed VPg (*v*irion *p*rotein *g*enome linked) is covalently linked to the 5′ end of all picornaviral RNAs (1, 28). Production of VPg-linked RNA is catalyzed by the viral polymerase 3Dpol in a two-step reaction. VPg or some precursor thereof is used to produce VPg-pUpU; VPg-pUpU is then used as a primer for production of full-length positive- or negative-sense RNA. A *cis*-acting replication element termed the "cre" or "oriI" is present at an internal position relative to the 5′ and 3′ ends of the picornaviral genome that is absolutely essential for genome replication (7, 9, 12, 16). Because *cis*-acting elements exist at the 5′ (oriL) and 3′ (oriR) ends of picornaviral genomes and the cre required for VPg is located at different positions in different PVs, herein we will use oriI to refer to the template for VPg uridylylation in order to preclude confusion as suggested by Paul (23).

oriI is an RNA stem-loop that has been shown to serve as an efficient template for production of VPg-pUpU in a 3Dpol-catalyzed reaction that is greatly stimulated by viral protein 3C or 3CD (22, 25, 27, 33). A single adenylate residue in the oriI loop serves as template for addition of both uridylate residues by using a slide-back mechanism similar to that observed in DNA phage phi29 (26). It is important to note that evaluation of VPg uridylylation in a cell-free system has shown that the cloverleaf (oriL) located in the 5′ untranslated region of picornaviral RNAs is required for VPg uridylylation (14). However, the function of the cloverleaf in VPg uridylylation is not clear (14). The suggestion has been made that this structure may facilitate delivery and/or activation of viral factors required for uridylylation (14). Consistent with this possibility is the fact that the use of processed proteins bypasses the dependence on the cloverleaf in vitro (22).

Our current model for the assembly and organization of the picornavirus VPg uridylylation complex is shown in Fig. 1 (21). This model is consistent with all of the currently available molecular genetic and biochemical studies performed to date in tissue culture, in cell-free systems, and in systems reconstituted from purified components (7, 18, 19, 21, 22, 24, 27, 30–33). A dimer of 3C(D) binds to oriI guided by an interaction between 3C and the upper stem of oriI. This complex isomerizes such that the upper stem opens to permit each of the single strands to interact with each 3C molecule. This isomerization is predicted to extend the loop into a conformation that will bind more readily to the RNA-binding site of 3Dpol (21), as suggested by structural studies of oriI (29). 3Dpol adds to this complex and is stabilized therein by an interaction between the back of the thumb of 3Dpol and a surface of the 3C dimer. VPg or some precursor thereof would

* Corresponding author. Mailing address: Pennsylvania State University, Department of Biochemistry and Molecular Biology, 201 Althouse Laboratory, University Park, PA 16802. Phone: (814) 863-8705. Fax: (814) 865-7927. E-mail: cec9@psu.edu.

† Present address: Department of Biomedical Sciences, Cornell University, Ithaca, NY 14853.

‡ Present address: Department of Molecular and Cellular Oncology, University of Texas M. D. Anderson Cancer Center, Houston, TX 77030.

§ Present address: Department of Medical Oncology, Fox Chase Cancer Center, Philadelphia, PA 19111.

▽ Published ahead of print on 12 September 2007.

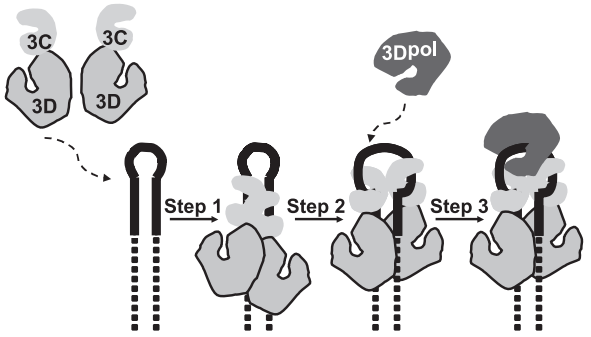

FIG. 1. Assembly and organization of the picornavirus VPg ribonucleoprotein complex. Step 1: two 3CD molecules bind to oriI with the 3C domains contacting the upper stem (solid lines) and the 3D domains contacting the lower stem (dashed lines). Step 2: the 3C dimer opens the RNA stem by forming a more stable interaction with single strands forming the stem. Step 3: 3Dpol is recruited to and retained in this complex by a physical interaction between the back of the thumb subdomain of 3Dpol and a surface of one or both 3C subdomains of 3CD.

either enter in association with 3Dpol (21) or join after 3Dpol binding. Although the catalytic sites for VPg-primed and RNA-primed RNA synthesis are the same, structural (6) and biochemical (11) studies suggest that the specific molecular interaction of nucleotide substrate with the 3Dpol active site is dependent on the primer employed. The overall organization of all picornavirus VPg uridylylation complexes will likely be similar. However, as suggested by the model, determinants for assembly and stability of this complex can be distributed across many protein-protein and protein-RNA interfaces.

oriI elements from human rhinovirus type 14 (HRV-14), poliovirus type 1 (PV-1), and PV-3 are shown in Fig. 2A. A loop consensus sequence has been defined (31). In contrast, a consensus sequence has not been defined for the stem, suggesting that only the structural stability of the stem is important for oriI function. Consistent with this possibility are two findings. First, a functional oriI has been created that contains a consensus loop in the context of a completely artificial stem (10). Second, PV-1 oriI can be replaced by the oriI element from HRV-14 without significant impact on replication efficiency (25). However, the observation that HRV-14 replication was impaired by using oriI from PV-3 suggested that protein factors might have undefined sequence-specific interactions with oriI (32). Consistent with this possibility was the finding that mutations in 3C and 3D coding sequence of HRV-14 could increase the efficiency of replication of an HRV-14 genome containing oriI from PV-3 (32). The mutation in 3C coding sequence changed Leu-94 to Pro; the mutation in 3D coding sequence changed Asp-406 to Asn. The mechanism(s) for adaptation is unknown.

We have established a VPg uridylylation system for HRV-14 that recapitulates biological phenotypes. We have discovered a previously unrecognized sequence specificity to the interaction between 3C and oriI that can be explained by a two-step binding mechanism that leads to unwinding of at least the upper stem of oriI. We show that 3C-L94P has a higher affinity for oriI RNAs that likely accounts for the expanded specificity of

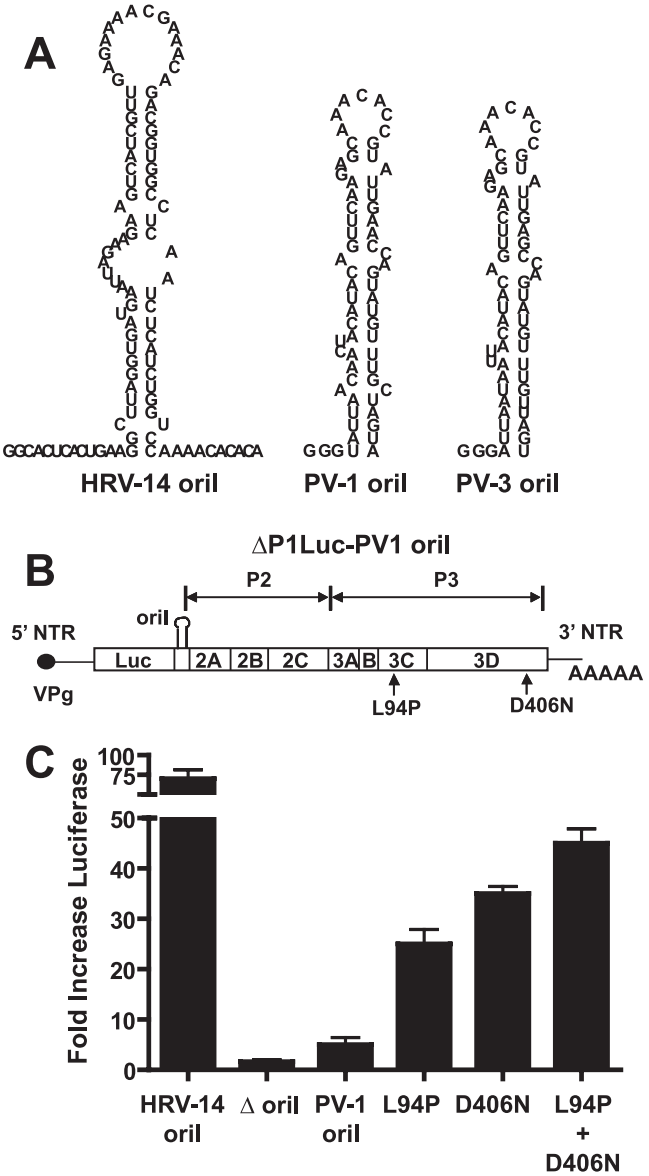

FIG. 2. Efficient PV-1-oriI-dependent replication of the HRV-14 genome requires adaptive mutations. (A) Secondary structures of HRV-14 oriI, PV-1 oriI, and PV-3 oriI predicted by the MFOLD RNA program. (B) Schematic of the subgenomic replicon ΔP1Luc-PV1 oriI. Most of the capsid protein sequence was replaced with the luciferase coding sequence, and the PV-1 oriI was inserted in frame between the luciferase and residual VP1 coding sequences at two engineered restriction sites, XhoI and NheI. NTR, nontranslated region. (C) 3C L94P and 3D D406N restore replication competence to the ΔP1Luc-PV1 oriI. The mutations of 3C L94P and 3D D406N were introduced into the ΔP1Luc-PV1 oriI replicon, and replication was monitored by assaying for luciferase after transfection of HeLa cells.

this variant that permits HRV-14 harboring this mutation to replicate by using PV-1 oriI. Surprisingly, the 3D-D406N mutation functions in 3Dpol rather than 3CD. 3Dpol-D406N assembles more readily and more stably in VPg uridylylation complexes by overcoming the destabilizing effect of nucleotide substitutions in oriI imposed by replacement of the native HRV-14 sequence with that of PV-1, thus permitting HRV-14

TABLE 1. Oligonucleotides used in this study

No.	Name	Sequence[a]
1	HRV-14-3C-SacII-F	5′-GCG **CCG CGG** TGG AGG CCA AGT AAT AGC TAG ACA T-3′
2	HRV-14-3C-BamHI-R	5′-GCG **GGA TCC** TTG TTT CTC TAC AAA ATA TTG TTT TTT AAG-3′
3	HRV-14-3C-L94P-F	5′-ATT TAT ATC AGA AGA TCc AGA AGG TGT GGA TGC C-3′
4	HRV-14-3C-L94P-R	5′-GGC ATC CAC ACC TTC TgG ATC TTC TGA TAT AAA T-3′
5	HRV-14-3C-C146G-F	5′-GCA ACA AAA ACT GGG CAG gGT GGA GGT GTG CTG TGT-3′
6	HRV-14-3C-C146G-R	5′-ACA CAG CAC ACC TCC ACc CTG CCC AGT TTT TGT TGC-3′
7	HRV-14-3D-SacII-F	5′-GCG **CCG CGG** TGG AGG CCA AGT AAT AGC TAG ACA T-3′
8	HRV-14-3D-NotI-R	5′-GCG **GCG GCC GCC** TCG AGT TAC TAA AAG AGG TCC AAC CAC CGC CT-3′
9	HRV-14-3D-BamHI-chis-R	5′-GCG GAA GAG CTC TTA CTA ATG GTG GTG ATG GTG GTG ACC AGA **GGA TCC** AAA GAG GTC CAA CCA GCG-3′
10	HRV-14-3D-D406N-F	5′-CAA TCA GAT GGA CAA AGa ATC CTA AAA ACA CAC AGG A-3′
11	HRV-14-3D-D406N-R	5′-TCC TGT GTG TTT TTA GGA TtC TTT GTC CAT CTG ATT G-3′
12	HRV-14-97nt-oriI-F	5′-CGG GAT CCT AAT ACG ACT CAC TAT AGG CAC TCA CTG AAG GCT TAG GT-3′
13	HRV-14-97nt-oriI-NheI-EcoRI-R	5′-GCG **GAA TTC GCT AGC** TGT GTG TTT TGG ACC AGA-3′
14	PV-3-oriI-BamHI-T7-F	5′-CG**G GAT CC**T AAT ACG ACT CAC TAT AGG GAT TAA TAA TTA CAT ACA-3′
15	PV-3-oriI-EcoRI-R	5′-GCG **GAA TTC** GCT AGC ACT AAC AAA CAT ACT GG-3′
16	PV-3D-KpnI-F	5′-GGC TGC TCA **GGT ACC** TCA ATT TTT AAC-3′
17	PV-3D-EcoRI-R	5′-GCG GGA TCC **GAA TTC** TTA CTA AAA TGA GTC AAG CCA ACG GC-3′
18	PV-3D-D406N-F	5′-CAA TTA GAT GGA CTA AAa ATC CTA GGA ACA CTC-3′
19	PV-3D-D406N-R	5′-GAG TGT TCC TAG GAT tTT TAG TCC ATC TAA TTG-3′

[a] Restriction sites are in boldface, nucleotide changes are in lowercase, and the T7 promoter is underlined.

to replicate by using PV-1 oriI. The two different mechanisms for adaptation are at least additive in vitro, providing an explanation for the additivity observed in tissue culture (32). These studies support and extend our understanding of the assembly and organization of the picornavirus VPg uridylylation complex. The biological implications of this new mechanistic insight are discussed.

MATERIALS AND METHODS

Materials. Deep Vent DNA polymerase and restriction enzymes were from New England Biolabs, Inc.; shrimp alkaline phosphatase was from USB; T4 DNA ligase was from Invitrogen Life Technologies; Difco-NZCYM was from BD Biosciences; QIAEX beads were from QIAGEN; RNase A was from Sigma; Ultrapure UTP solution was from GE Healthcare; [α-^{32}P]UTP (6,000 Ci/mmol) was from Perkin-Elmer Life Sciences, Inc.; synthetic PV and HRV-14 VPg peptides were purchased from Alpha Diagnostic International (San Antonio, TX); all other reagents and apparatuses were available through Fisher or VWR or as indicated.

Cloning and transcription of HRV-14, PV-3, and HRV-14/PV-3 chimeric oriIs. Cloning and transcription of PV-1 61-nucleotide (nt) oriI were performed as described previously (22). DNA fragments carrying HRV-14 97-nt oriI were generated by PCR amplification using oligonucleotides 12 and 13 (Table 1) and cloned into a pUC18 vector using BamHI and EcoRI sites. Transcription reactions were performed as described for PV 61-nt oriI (22). The extinction coefficient for HRV-14 97-nt oriI was 1.1328 $\mu M^{-1} \cdot cm^{-1}$. The plasmids ΔP1Luc-PV3 oriI, ΔP1Luc-PV lp, and ΔP1Luc-PV stem were constructed as described previously (32). DNA fragments carrying PV-3 oriI, PV-3 stem (HRV-14 loop), and PV-3 lp (HRV-14 stem) were generated by PCR amplification with replicons of ΔP1Luc-PV3 oriI, ΔP1Luc-PV lp, or ΔP1Luc-PV stem as templates using oligonucleotides 14 and 15 and oligonucleotides 12 and 13 (Table 1). Transcription reactions were performed as described previously for PV 61-nt oriI (22). The extinction coefficients for PV-3 oriI, PV-3 stem, and PV-3 lp were 0.7841, 0.7511, and 1.1613 $\mu M^{-1} \cdot cm^{-1}$, respectively.

Construction of pET26Ub HRV-14 3D WT and 3D D406N. For 3D wild type (WT), a PCR fragment was made with HRV-14 viral cDNA (15) as a template using oligonucleotides 7 and 8 as primers (Table 1). For 3D D406N, first two PCR fragments were amplified using oligonucleotides 7 and 8 and oligonucleotides 10 and 11 (Table 1) encoding point mutation D406N. These two fragments were then used as templates for the amplification of a new fragment using oligonucleotides 7 and 8 (Table 1). The PCR products of 3D WT and 3D D406N were cloned into pET26Ub using SacII and XhoI sites.

Construction of pET26Ub HRV-14 3C WT and 3C L94P. Oligonucleotides 1 and 2 (Table 1) were used to amplify 3C WT. For 3C L94P, first two PCR fragments were amplified using oligonucleotides 1 and 4 and oligonucleotides 3 and 2 (Table 1) encoding point mutation L94P. These two fragments were then used as templates for the amplification of a new fragment using oligonucleotides 1 and 2 (Table 1). The PCR products of 3C WT and 3C L94P were cloned into pET26Ub-Chis plasmid using SacII and BamHI sites. pET26Ub-Chis is designed to produce a C-terminal GSSG–six-His tag for any protein coding sequence cloned in by using the 3′ BamHI1 site.

Construction of pET26Ub HRV-14 3CD and 3CD derivatives. pET26Ub 3CD Chis was made the same way as described for pET26Ub 3C Chis. Three 3CD mutants, 3C*D (3C-L94P-D), 3CD* (3CD-D406N), and 3C*D* (3C-L94P-D-D406N), were made by PCR mutagenesis as described above. Oligonucleotides 1, 3, 4, and 8 were used for 3C*D; oligonucleotides 1 and 9 to 11 were used for 3CD*; and oligonucleotides 1, 3, 4, and 9 to 11 were used for 3C*D* PCR amplifications. All plasmids contain a mutation of cysteine 146 to a glycine to inactivate protease activity.

Construction of pET26Ub PV 3D D406N. pET26Ub PV 3D-D406N was constructed as described previously for 3D WT (8). Oligonucleotides 16 to 19 (Table 1) were used for the PCR amplifications. The PCR products were cloned into pET26Ub 3D WT using KpnI and EcoRI sites.

Expression and purification of HRV-14 3D polymerase. *Escherichia coli* Rosetta pUbpS was transformed with pET26Ub HRV-14 3D WT or 3D D406N for protein expression. The strain Rosetta pUbpS carries the pUbpS plasmid, which constitutively expresses a yeast ubiquitin protease that processes the ubiquitin fusion protein to produce the authentic N terminus. Protein expression, precipitation of nucleic acid with polyethyleneimine, and ammonium sulfate precipitation were performed as previously described (22). The ammonium sulfate pellet was resuspended in buffer A (50 mM Tris, pH 8.0, 0.1% Nonidet P-40, 20% glycerol, 10 mM β-mercaptoethanol) containing 150 mM NaCl and dialyzed against 1000 ml of dialysis buffer (buffer A with 150 mM NaCl) at 4°C overnight. After dialysis, the protein was adjusted to 50 mM NaCl and loaded at the speed of 1 ml/min onto a phosphocellulose (P-11) column equilibrated with buffer A containing 50 mM NaCl. Proteins were eluted with a gradient from 50 to 350 mM NaCl in buffer A. The eluted pooled fractions were loaded to a Q-Sepharose column as described for the P-11 column. The eluted fractions were adjusted with buffer A to 50 mM NaCl and loaded onto a 0.5-ml Q column, which was equilibrated with buffer A containing 50 mM NaCl. After loading, the column was washed with buffer B (50 mM HEPES, pH 7.5, 0.1% Nonidet P-40, 20% glycerol, 10 mM β-mercaptoethanol) containing 50 mM NaCl. Proteins were eluted with buffer B containing 500 mM NaCl and dialyzed against 1,000 ml of buffer B containing 50 mM NaCl at 4°C overnight. The protein concentration was

determined at 280 nm in 6 M guanidine HCl, pH 6.5, using the extinction coefficient 0.0585 $\mu M^{-1} \cdot cm^{-1}$.

Expression and purification of PV 3D polymerase. Expression and purification of PV 3Dpol were performed as previously described (8).

Expression and purification of HRV-14 3C WT and 3C L94P. The BL21(DE3) pCG1 strain of *E. coli* was transformed with pET26Ub HRV-14 3C six-His for protein expression. The protein expression, lysis, and polyethyleneimine and ammonium sulfate precipitation were performed as previously described (22), except that 60% ammonium sulfate precipitation was employed. The ammonium sulfate pellet was resuspended in buffer A (50 mM Tris, pH 8.0, 0.1% Nonidet P-40, 20% glycerol, 10 mM β-mercaptoethanol) containing 500 mM NaCl and dialyzed against 1000 ml of dialysis buffer (buffer A with 500 mM NaCl) at 4°C overnight. After dialysis, the protein was adjusted to 500 mM NaCl and loaded onto a Ni-nitrilotriacetic acid-agarose column at the flow rate of 1 ml/min. The column was washed with 6× column volumes of buffer A containing 500 mM NaCl and 50 mM imidazole. Proteins were eluted with 2 M NaCl in buffer A containing 500 mM imidazole. The eluted pooled fractions were adjusted with buffer A to 50 mM NaCl and were purified using a phosphocellulose (P-11) column as described for HRV-14 3D purification. The protein concentration was determined at 280 nm in 6 M guanidine HCl, pH 6.5, using the extinction coefficient 0.0051 $\mu M^{-1} \cdot cm^{-1}$.

Expression and purification of HRV-14 3CD WT and 3CD derivatives. The BL21(DE3)pCG1 strain of *E. coli* was transformed with pET26Ub HRV-14 3CD six-His for protein expression. The protein expression, lysis, and polethyleneimine and ammonium sulfate precipitation were performed as previously described (22). The ammonium sulfate pellet was resuspended in lysis buffer (100 mM potassium phosphate, pH 8.0, 0.1% Nonidet P-40, 20% glycerol, 10 mM β-mercaptoethanol, 500 mM NaCl, 2.8 μg/ml pepstatin A, 2.0 μg/ml leupeptin, 2 mM phenylmethylsulfonyl fluoride). The protein was loaded onto a Ni-nitrilotriacetic acid-agarose column at the flow rate of 1 ml/min. The column was washed with buffer B (50 mM HEPES, pH 7.5, 0.1% Nonidet P-40, 20% glycerol, 10 mM β-mercaptoethanol) containing 500 mM NaCl and 20 mM imidazole. Proteins were eluted with 500 mM NaCl in buffer B containing 500 mM imidazole. The eluted pooled fractions were dialyzed against 1,000 ml of dialysis buffer (buffer B with 150 mM NaCl) at 4°C overnight. After dialysis, the protein was adjusted to 50 mM NaCl and loaded at the speed of 1 ml/min onto a phosphocellulose (P-11) column equilibrated with buffer B containing 50 mM NaCl and eluted with buffer B containing 500 mM NaCl. The eluted pooled fractions were dialyzed against buffer B containing 150 mM NaCl at 4°C overnight. The protein concentration was determined at 280 nm in 6 M guanidine HCl, pH 6.5, using the extinction coefficient 0.0636 $\mu M^{-1} \cdot cm^{-1}$.

Subgenomic replicon assays. Subgenomic HRV-14 replicons were constructed as described previously (32). RNAs transcribed in vitro from these constructs were transfected into HeLa cells, which were seeded into six-well plates, and cultured in Dulbecco modified Eagle medium with 10% fetal bovine serum at 34°C. Cell lysates were harvested by the addition of 125 ml of passive lysis buffer (Promega) to each well and stored at −70°C until assayed for enzymatic activity. Luciferase activity was quantified using the Luciferase Assay System as described by the supplier (Promega), and the results were determined using a TD-20/20 luminometer (Turner Designs).

VPg uridylylation assays. The reaction mixture contained 1 μM 3C or 3CD, 1 μM HRV-14 97-nt oriI or PV 61-nt oriI, and 10 μM VPg in reaction buffer (50 mM HEPES, pH 7.5, 5 mM magnesium acetate, 10% glycerol, 10 mM β-mercaptoethanol, 0.04 μM [α-^{32}P]UTP [6,000 Ci/mmol], and 10 μM unlabeled UTP). The reaction mixture was preheated at 30°C for 5 min. Reactions were initiated with 3D (10 μM for HRV-14 or 1 μM for PV). All enzymes were diluted immediately prior to use in enzyme dilution buffer (50 mM HEPES, pH 7.5, 10 mM β-mercaptoethanol, 20% glycerol). After incubation at 30°C for 30 min, the reaction was then stopped by the addition of an equal volume (5 μl) of gel loading buffer (100 mM EDTA in 75% formamide, 0.025% bromophenol blue, and 0.025% xylene cyanol). The quenched samples (5 μl) were analyzed by Tris-Tricine sodium dodecyl sulfate (SDS)-polyacrylamide gel electrophoresis. The incorporation of [α-^{32}P]UMP was measured on a PhosphorImager and quantified by using ImageQuant software. The concentration of VPg extended was calculated using values for the counts associated with the indicated components in the equation [(VPg-pU + VPg-pUpU/2)/(VPg-pU + VPg-pUpU/2 + UTP)] × [UTP]. The processivity of the reaction is defined as follows: [VPg-pUpU]/[VPg-pUpU] + [VPg-pU].

RNA filter binding assays. For direct binding experiments, the reaction mixture (20 μl) contained 10 nM trace-labeled HRV-14 97-nt oriI or PV-1 61-nt oriI and various concentrations of WT HRV-14 3C. For competitive binding experiments, the reaction mixture (20 μl) contained 10 nM trace-labeled HRV-14 97-nt oriI and various concentrations of unlabeled PV 61-nt oriI or unlabeled HRV-14 97-nt oriI. In all cases, the reaction buffer contained 50 mM HEPES (pH 7.5), 20 mM NaCl, 5 mM magnesium acetate, 20% glycerol, and 10 mM β-mercaptoethanol. The binding reactions were initiated with 0.03 μM 3C, and the reaction mixtures were incubated at 30°C for 15 s (direct binding) or 15 min (competitive binding). 3C was diluted immediately prior to use in enzyme dilution buffer as described above. Three filters were employed, and the filter binding assays were performed as previously described (22).

Poly(rU) polymerase activity. The reaction mixture (25 μl) contained 0.5 μM 3Dpol, 2 μM dT_{15}, 0.2 μM poly(rA)$_{467}$, 500 μM UTP, and 0.4 μCi/μl [α-^{32}P]UTP in enzyme buffer (50 mM HEPES, pH 7.5, 5 mM NaCl, 5 mM $MgCl_2$, 20% glycerol, and 10 mM β-mercaptoethanol). Experiments were performed at 30°C and initiated with 3Dpol. After 5 min of incubation, the reactions were quenched by addition of EDTA to a final concentration of 50 mM. Five microliters of quenched reaction was spotted onto Whatman DE-81 filter paper. Dried filter paper was washed three times with 5% (wt/vol) dibasic sodium phosphate. Bound radioactivity was quantified by liquid scintillation counting.

Rapid chemical quench flow experiments. Experiments were performed at 30°C by using a circulating water bath and using a model RQF-3 chemical quench flow apparatus (KinTek Corp., State College, PA) (3, 4). 3Dpol and sym/sub were mixed for 3 min at room temperature, and then the 3Dpol-sym/sub complexes were rapidly mixed with the nucleotide substrate. The reactions were quenched by adding EDTA to a final concentration of 0.3 M.

RESULTS

Efficient PV-1 oriI-dependent replication of the HRV-14 genome requires adaptive mutations. There are differences in the sequence of the lower stem of PV-1 oriI relative to PV-3 oriI (Fig. 2A). Because HRV-14 oriI could be used by PV-1, it was important to show that the inability of PV-3 oriI to substitute for HRV-14 oriI was not caused by the observed sequence differences. These studies employed an HRV-14 subgenomic replicon whose replication could be monitored by measuring luciferase activity (Fig. 2B) (32). In this system, HRV-14 oriI yielded an increase in luciferase activity 50- to 100-fold higher than that of a replicon lacking oriI (Fig. 2C) (32). Addition of PV-1 oriI to the HRV-14 replicon containing the oriI deletion did not restore replication to the level observed for HRV-14 oriI (Fig. 2C). Importantly, adaptive mutations in 3C (L94P) and 3D (D406N) isolated by using PV-3 oriI also increased utilization of PV-1 oriI (Fig. 2C). As observed previously (32), the two adaptive mutations were at least additive, possibly synergistic (Fig. 2C), suggesting independent mechanisms for the adaptive mutations.

PV-1 oriI does not substitute for HRV-14 oriI in vitro. VPg uridylylation has been reconstituted in vitro from purified components for a variety of picornaviruses (7, 25), but a system to study HRV-14 VPg uridylylation has not been developed. Reconstitution of HRV-14 VPg uridylylation in vitro would facilitate determination of how the adaptive changes in 3C and 3D coding sequence permit utilization of PV-1 oriI, providing additional insight into the mechanism of this key step in picornavirus genome replication.

We have expressed and purified HRV-14 3C, 3Dpol, and 3CD (Fig. 3A) by using the pET-ubiquitin system and purification schemes described previously for the analogous PV-1 proteins (8). Production of VPg-pU(pU) was observed in a reconstituted in vitro VPg uridylylation reaction containing HRV-14 3Dpol, 3C(D), VPg, and HRV-14 oriI (Fig. 3B). This reaction was linear for at least 2 hours (Fig. 3C). We were unable to chase the VPg-pU product formed into VPg-pUpU product over time (data not shown), suggesting that once VPg-pU dissociates, rebinding of this product in a productive conformation may not occur. Importantly, PV-1 oriI was not

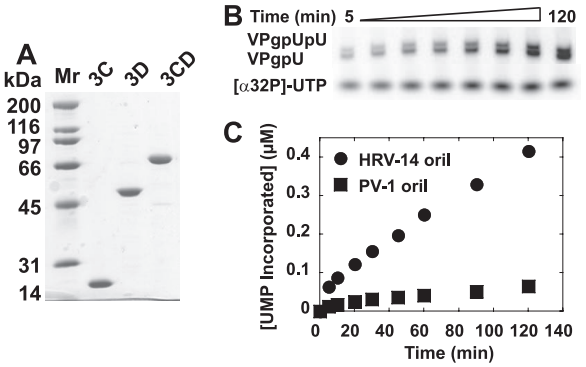

FIG. 3. Reconstitution of HRV-14 VPg uridylylation in vitro from purified components. (A) Purified proteins employed in this experiment. Two micrograms of each protein was analyzed by 10% SDS-polyacrylamide gel electrophoresis. The gels were stained with Coomassie brilliant blue R-250. (B) VPg uridylylation reaction product analysis. VPg uridylylation reaction mixtures contained WT 3D (10 μM), WT 3CD (1 μM), HRV-14 97-nt oriI (1 μM), and 10 μM VPg in reaction buffer (50 mM HEPES, pH 7.5, 5 mM magnesium acetate, 10% glycerol, 10 mM β-mercaptoethanol, 0.04 μM [α-^{32}P]UTP [6,000 Ci/mmol], and 10 μM unlabeled UTP). The quenched samples were analyzed by Tris-Tricine-SDS-polyacrylamide gel electrophoresis. The phosphorimage of the gel is shown. A time-dependent increase in formation of VPg-pU(pU) was observed. (C) HRV-14 oriI functions better than PV-1 oriI in VPg uridylylation reaction mixtures containing HRV-14 proteins. Reactions were performed as described above by using either 1 μM HRV-14 97-nt oriI (●) or 1 μM PV-1 61-nt oriI (■). ImageQuant software was used to quantify VPgpU(pU) formed. These data were plotted as a function of time. The kinetics of product formation were linear for at least 2 h, thus validating the use of a 30-min time point for comparison of oriI utilization.

an efficient template for VPg uridylylation catalyzed by using HRV-14 replication proteins (Fig. 3C), consistent with observations made in tissue culture (Fig. 2C).

The adaptive mutation in 3D functions in 3Dpol, and the adaptive mutation in 3C functions in 3C(D). Although the adaptive mutation in 3C was likely to function in 3C(D), it was not clear whether the adaptive mutation in 3D functioned in 3CD or 3Dpol. In order to address this question, we engineered the adaptive mutations individually or in combination into expression vectors for 3C, 3CD, and/or 3Dpol. These derivatives were expressed and purified as described for the corresponding WT proteins. The quality of these proteins was on par with that of the WT proteins (data not shown). When the 3D-D406N substitution was present in 3CD (site of mutation denoted by asterisk in figures), stimulation of VPg uridylylation was not observed when either HRV-14 oriI or PV-1 oriI was employed as template (bars 2 and 8 of Fig. 4A). A twofold reduction was noted that could be alleviated by increasing the concentration of 3CD-D406N employed in the reaction (data not shown). However, when the 3D-D406N substitution was present in 3Dpol, at least a fivefold increase in VPg uridylylation was observed when HRV-14 oriI and PV-1 oriI were employed as templates (bars 3 and 9 of Fig. 4A). Importantly, the level of VPg uridylylation observed for 3Dpol-D406N with PV-1 oriI as template was equivalent to that observed for WT 3Dpol with HRV-14 oriI (compare bar 9 and bar 1 of Fig. 4A). The combination of 3CD with the adaptive change and

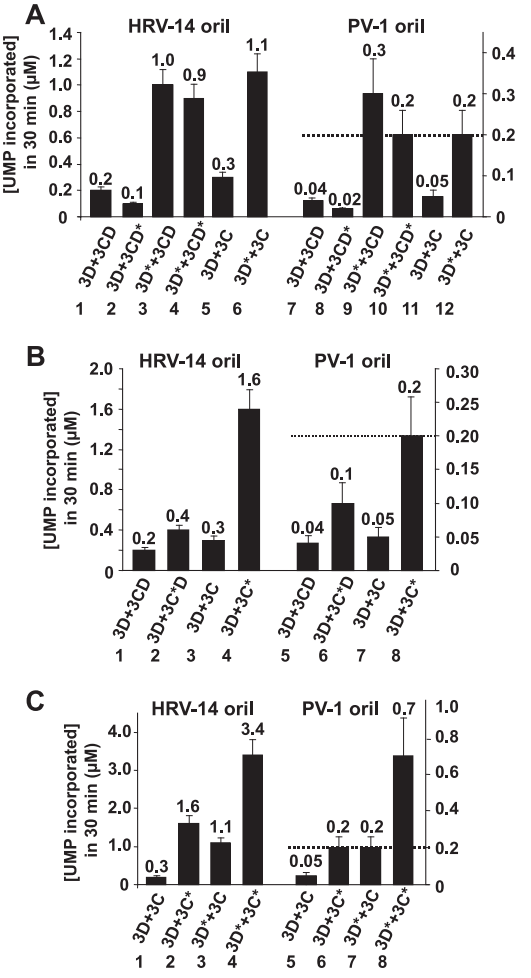

FIG. 4. Characterization of 3C, 3CD, and/or 3D proteins containing adaptive changes. HRV-14 VPg uridylylation reactions were performed with either HRV-14 oriI or PV-1 oriI and the indicated HRV-14 proteins. VPg uridylylation reaction mixtures contained WT or D406N (D*) 3Dpol (10 μM), WT or L94P (C*) 3C or 3CD (1 μM), HRV-14 97-nt oriI or PV-1 61-nt oriI (1 μM), and 10 μM VPg in reaction buffer (50 mM HEPES, pH 7.5, 5 mM magnesium acetate, 10% glycerol, 10 mM β-mercaptoethanol, 0.04 μM [α-^{32}P]UTP [6,000 Ci/mmol], and 10 μM unlabeled UTP). Shown is the concentration of [α-^{32}P]UMP incorporated into VPgpU(pU) in 30 min at 30°C. The dotted lines indicate the level of UMP incorporated (0.2 μM) in 30 min in a reaction employing WT HRV-14 3D, WT HRV-14 3CD, and HRV-14 oriI. We assume that a value of 0.2 μM corresponds to a value sufficient to support virus replication. (A) HRV-14 3D D406N improves utilization of HRV-14 and PV-1 oriI only in the context of 3Dpol and not in 3CD. The ability of 3D* or 3CD* to improve utilization of PV-1 oriI was determined by performing VPg uridylylation reactions as described above. (B) HRV-14 3C L94P improves utilization of PV-1 oriI in the context of 3CD and 3C. The ability of 3C* or 3C*D to improve utilization of PV-1 oriI was determined by performing VPg uridylylation reactions as described above. (C) 3D-D406N and 3C-L94P function by independent mechanisms. VPg uridylylation reactions were performed as described above to determine the effect of combining 3C* and 3D* on PV-1 utilization. The assumption here is that if the molecular mechanism for adaptation of the two proteins is the same, then the combination would be less than additive or even antagonistic. However, independent mechanisms should lead to an additive or synergistic increase in product formation. The combination was at least additive, possibly synergistic.

TABLE 2. PV-1 3Dpol-D406N exhibits a specific increase in VPg uridylylation activity

PV 3Dpol derivative	AMP incorporation (s^{-1})		Activity	
	Steady state	Pre-steady state	Poly(rU) polymerase (pmol/min/μg)	VPg uridylylation (μM UMP incorporated/min)
WT	$(2.77 \pm 0.18) \times 10^{-4}$	69.0 ± 1.5	190 ± 8	0.03 ± 0.01
D406N	$(2.80 \pm 0.22) \times 10^{-4}$	63.8 ± 1.3	215 ± 6	0.11 ± 0.03

3Dpol-D406N did not show any additional stimulation (bars 4 and 10 of Fig. 4A). In this system, 3C and 3CD were indistinguishable (for example, compare bar 1 to bar 5 and bar 7 to bar 11 in Fig. 4A). These data are consistent with the adaptive mutation in 3D coding sequence functioning at the level of 3Dpol, not 3CD. Importantly, the increased activity of the 3Dpol-D406N derivative was not restricted to the heterologous PV-1 oriI but was observed with the cognate HRV-14 RNA element as well. This observation suggests that its increased activity is not dependent upon specific sequence or structure differences in oriI; however, the increased VPg uridylylation activity of this derivative was not merely due to a change in polymerase activity, as the two enzymes exhibited equivalent poly(rU) polymerase activities (data not shown).

By performing a comparable set of experiments with the 3C-L94P derivative, it was made clear that 3C-L94P functioned in 3C(D), causing at least a fivefold stimulation in VPg uridylylation in reactions templated by either HRV-14 oriI or PV-1 oriI (compare bar 3 to bar 4 and bar 7 to bar 8 in Fig. 4B). The solubility of 3CD-L94P was reduced relative to that of WT 3CD, leading to a lower concentrations of the protein stock, a higher concentration of detergent in the reaction mixture, and attenuation of the stimulatory activity of 3CD-L94P on VPg uridylylation (compare bar 2 to bar 4 and bar 6 to bar 8 in Fig. 4B; also data not shown).

The combination of 3Dpol-D406N and 3C-L94P in reactions templated by either HRV-14 oriI or PV-1 oriI was at least additive, possibly synergistic (Fig. 4C). This observation is consistent with observations made with chimeric replicon RNAs in cell culture (Fig. 2C) (32) and suggests that the two mutations function by independent mechanisms. We conclude that the in vitro HRV-14 VPg uridylylation system recapitulates biological phenotypes and thus can be used to define biologically relevant mechanisms.

PV-1 3Dpol-D406N exhibits a specific increase in VPg uridylylation activity. HRV-14 3Dpol did not assemble readily on the synthetic primed-template substrate (sym/sub) designed for mechanistic studies of PV-1 3Dpol (data not shown) (2). In order to prove that the D406N change did not function by changing a more general activity of 3Dpol, we engineered this substitution into PV-1 3Dpol. PV-1 3Dpol-D406N was fourfold more efficient than WT 3Dpol at VPg uridylylation (Table 2). Significant differences were not observed in the poly(rU) polymerase activity, pre-steady-state rate constant for single nucleotide (AMP) incorporation, or steady-state rate constant for AMP incorporation (Table 2). We conclude that the gain of function associated with the D406N substitution is unique to the VPg uridylylation reaction and is not caused by some indirect effect on polymerase activity.

3Dpol-D406N is recruited to and retained in VPg uridylylation complexes more efficiently than WT 3Dpol. In order to determine the mechanistic basis for the increased VPg uridylylation activity of 3Dpol-D406N relative to WT 3Dpol, we titrated each of the HRV components in reactions as follows: HRV-14 oriI (Fig. 5A), HRV-14 3C (Fig. 5B), and HRV-14 VPg (Fig. 5C). The data were evaluated in two ways. First, the amount of VPg extended was plotted as a function of the concentration of the indicated reaction component, and the data were fitted to a hyperbolic equation, yielding values for the maximal amount of VPg extended and a $K_{0.5}$ value for the titrated component. The maximal amount of VPg extended

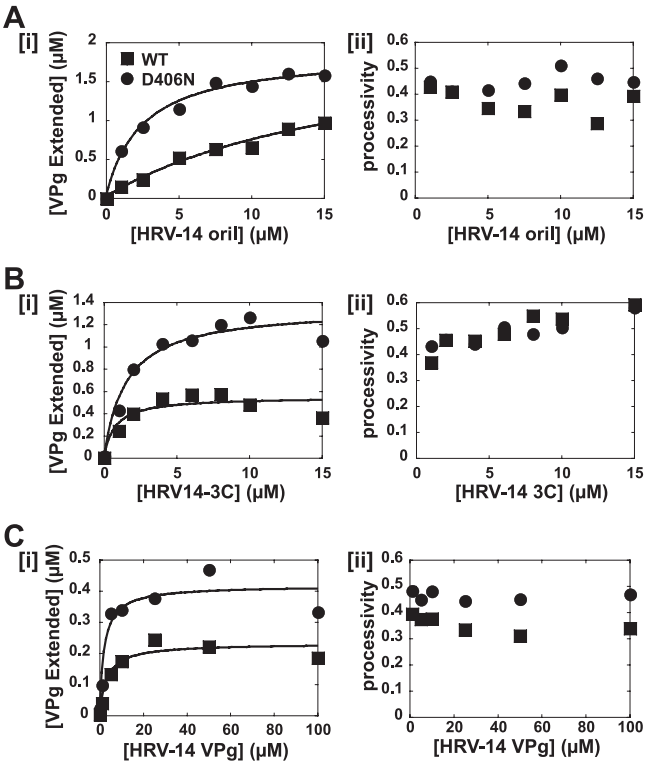

FIG. 5. 3Dpol-D406N is recruited to and retained in VPg uridylylation complexes more efficiently than WT 3Dpol. The uridylylation reactions were performed as described in Materials and Methods. The amount of VPg extended (i) or processivity (ii) was plotted as a function of oriI, 3C, or VPg concentration. ■, HRV-14 3D WT; ●, HRV-14 3D D406N. (A) HRV-14 oriI was titrated from 0 to 15 μM in the uridylylation reaction mixtures containing HRV-14 3D WT or 3D D406N. The solid lines represent the fit of the data to a hyperbolic equation with a $K_{0.5}$ of 16.2 ± 5.6 μM for 3D WT and 2.4 ± 0.4 μM for 3D D406N and endpoints of 1.84 ± 0.10 μM for 3D WT and 2.1 ± 0.62 μM for 3D D406N. (B) HRV-14 3C was titrated from 0 to 15 μM in the reaction mixtures containing HRV-14 3D WT or 3D D406N. The solid lines represent the fit of the data to a hyperbolic equation with a $K_{0.5}$ of 1.0 ± 0.5 μM for 3D WT and 1.3 ± 0.2 μM for 3D D406N and endpoints of 0.55 ± 0.11 μM for 3D WT and 1.35 ± 0.13 μM for 3D D406N. (C) HRV-14 VPg was titrated from 0 to 100 μM in the reaction mixtures containing HRV-14 3D WT or 3D D406N. The solid lines represent the fit of the data to a hyperbolic equation with a $K_{0.5}$ of 3.8 ± 0.5 μM for WT 3D and 2.0 ± 0.5 μM for 3D D406N and endpoints of 0.23 ± 0.03 μM for WT 3D and 0.41 ± 0.06 μM for 3D D406N.

should correlate directly with the number of uridylylation complexes that form—that is, recruitment of the static component. The $K_{0.5}$ value for the titrated component should provide a measure of affinity (recruitment) and stability (retention) of this component for the uridylylation complex. Second, we plotted the processivity of VPg uridylylation—that is, the amount of VPg-pUpU formed relative to the sum of VPg-pUpU and VPg-pU. Increased processivity should correlate directly with the retention of the static component in the VPg uridylylation complex. A significant difference ($P < 0.05$) in processivity occurred when values obtained in an experiment performed at the same time differed by more than 10%.

In all cases, 3Dpol-D406N extended more VPg molecules than WT 3Dpol (panels i of Fig. 5A, B, and C). We interpret this to mean that 3Dpol-D406N was recruited more efficiently to the VPg uridylylation complex. The $K_{0.5}$ value of 3Dpol-D406N for HRV-14 oriI was reduced eightfold relative to WT (panel i of Fig. 5A). Because the active form of oriI is a $3C_2$-oriI complex (21), we conclude that 3Dpol-D406N is recruited to the $3C_2$-oriI complex more efficiently. A significant difference in the $K_{0.5}$ values for HRV-14 3C and HRV-14 VPg was not observed (panel i of Fig. 5B and C, respectively). A difference was not expected as the $K_{0.5}$ value of 3C likely measures affinity for RNA (21) and the $K_{0.5}$ value of VPg likely measures affinity for the 3Dpol RNA-binding site, which is remote from amino acid 406 (13).

Although more VPg uridylylation complexes formed by using 3Dpol-D406N as the concentration of HRV-14 VPg increased, the processivity of these complexes was unchanged relative to WT (panel ii of Fig. 5C), again consistent with enhanced recruitment of this derivative to the VPg uridylylation complex rather than retention therein. A systematic increase in processivity of equivalent magnitude was observed for both 3Dpol and 3Dpol-D406N VPg uridylylation complexes as the concentration of HRV-14 3C was increased (panel ii of Fig. 5B). This observation would suggest that a 3Dpol-VPg-pU complex can rebind to the $3C_2$-oriI complex if the kinetics of $3C_2$-oriI assembly are faster than dissociation of VPg-pU from 3Dpol. Interestingly, at saturating concentrations of HRV-14 VPg, the processivity of 3Dpol-D406N (0.41 ± 0.03) was greater than that of WT 3Dpol (0.33 ± 0.03), suggesting that 3Dpol-D406N was retained in the VPg uridylylation complex more efficiently than WT 3Dpol (panel ii of Fig. 5C).

3C-L94P assembles with oriI more efficiently and more stably than WT 3C. The adaptive change in 3C was evaluated as described above for 3Dpol (Fig. 6). The maximal amount of VPg extended in the presence of 3C-L94P was fourfold greater than that observed for 3C when HRV-14 oriI was employed (panel i of Fig. 6A and B), suggesting that 3C-L94P was more efficient at forming productive $3C_2$-oriI complexes. Consistent with this conclusion was the finding that the $K_{0.5}$ value for oriI was reduced by 8- to 10-fold by using 3C-L94P instead of 3C (panel i of Fig. 6A and B). A change in processivity was not observed (panel ii of Fig. 6A and B).

3C-L94P also formed more productive complexes with PV-1 oriI than WT 3C as the amount of VPg extended was increased due to a decrease in the $K_{0.5}$ value for PV-1 oriI (panel i of Fig. 6C and D). Complexes with the 3C derivative were also more

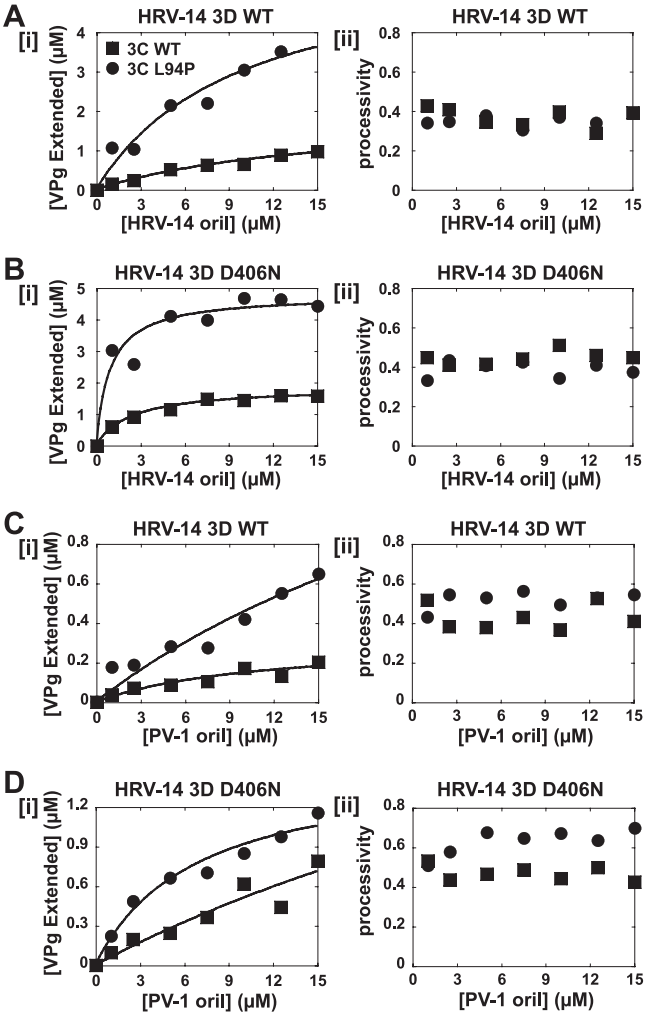

FIG. 6. 3C-L94P assembles with oriI more efficiently and more stably than WT 3C. The uridylylation reactions were performed as described in Materials and Methods. HRV-14 oriI or PV-1 oriI was titrated from 0 to 15 μM in the reaction mixtures containing either HRV-14 3D WT or 3D D406N and either HRV-14 3C WT or 3C L94P. The amount of VPg extended (i) or processivity (ii) was plotted as a function of oriI concentration. ■, HRV-14 3C WT; ●, HRV-14 3C L94P. (A) Titration of HRV-14 oriI with HRV-14 3D WT and either HRV-14 3C WT or 3C L94P. The solid lines represent the fit of the data to a hyperbolic equation with a $K_{0.5}$ of 16.2 ± 5.6 μM for 3C WT and 9.8 ± 5.4 μM for 3C L94P and endpoints of 2.10 ± 0.62 μM for 3C WT and 6.01 ± 1.78 μM for 3C L94P. (B) Titration of HRV-14 oriI with HRV-14 3D D406N and either HRV-14 3C WT or 3C L94P. The solid lines represent the fit of the data to a hyperbolic equation with a $K_{0.5}$ of 2.4 ± 0.4 μM for 3C WT and 0.94 ± 0.34 μM for 3C L94P and endpoints of 1.84 ± 0.10 μM for 3C WT and 4.78 ± 0.34 μM for 3C L94P. (C) Titration of PV-1 oriI with HRV-14 3D WT and either HRV-14 3C WT or 3C L94P. The solid lines represent the fit of the data to a hyperbolic equation with a $K_{0.5}$ of 95 ± 10 μM for 3C WT and 22.5 ± 2.0 μM for 3C L94P and endpoints of 1.5 μM for both 3C WT and 3C L94P. (D) Titration of HPV-1 oriI with HRV-14 3D D406N and either HRV-14 3C WT or 3C L94P. The solid lines represent the fit of the data to a hyperbolic equation with a $K_{0.5}$ of 19.0 ± 2.3 μM for 3C WT and 6.4 ± 0.5 μM for 3C L94P and endpoints of 1.5 μM for both 3C WT and 3C L94P.

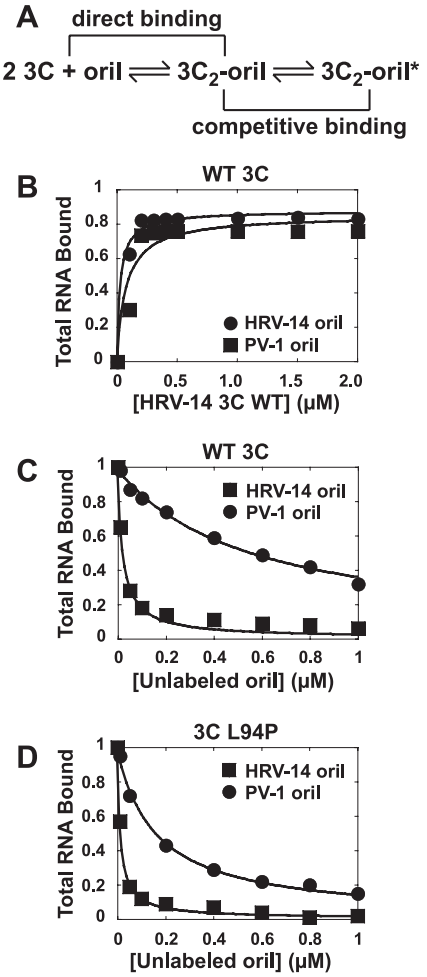

FIG. 7. Two-step mechanism for 3C binding to oriI. (A) Two 3C molecules bind to oriI to form a ground-state complex ($3C_2$-oriI). This complex isomerizes into a more stable activated complex (3C-oriI*) competent for recruitment of polymerase and uridylylation. The isomerization step is slow; therefore, when a filter binding experiment is performed with a short incubation time, the assay reports on the formation of the initial ground-state complex (direct binding). When the binding reaction is allowed to proceed for longer times, as in the case for the competitive binding experiments, the assay reports on the formation of the isomerized complex (competitive binding). (B) Direct binding experiment. Radiolabeled HRV-14 oriI or PV-1 oriI was mixed with various concentrations of HRV-14 3C WT for 15 s at 30°C. Quantification of the protein-RNA complexes was determined by using a direct filter binding assay. A slot blot apparatus was used in this experiment as described in Materials and Methods. The polysulfone and nitrocellulose membranes bind protein-RNA complex and free protein, and the nylon membrane binds all of the free RNA. ●, HRV-14 oriI; ■, PV-1 oriI. Quantification of the protein-RNA complexes on the polysulfone and nitrocellulose membranes shows binding of HRV-14 oriI and PV-1 oriI to HRV-14 3C. The solid lines represent the fit of the data to a hyperbolic equation with a $K_{0.5}$ of 0.029 ± 0.007 μM for HRV-14 oriI and 0.078 ± 0.034 μM for PV-1 oriI. (C) Competitive binding experiment. Radiolabeled HRV-14 oriI was mixed with various concentrations of unlabeled HRV-14 oriI or PV-1 oriI and incubated with 0.3 μM HRV-14 3C WT for 15 min at 30°C. Quantification of the protein-RNA complexes was determined by using a filter binding assay. A slot blot apparatus was used in this experiment as described in Materials and Methods. The polysulfone and nitrocellulose membranes bind protein-RNA complex and free protein, and the nylon membrane binds all of the free RNA. ●, unlabeled PV-1 oriI; ■, unlabeled HRV-14 oriI. Quantification of the protein-RNA complexes on the polysulfone and nitrocellulose membranes shows binding competence between HRV-14 oriI and PV-1 oriI to HRV-14 3C. The solid lines represent the fit of the data to a hyperbolic equation with a 50% inhibitory concentration of 0.02 ± 0.003 μM for HRV-14 oriI and 0.56 ± 0.03 μM for PV-1 oriI. (D) 3C-L94P exhibits a higher affinity for PV-1 oriI relative to WT 3C. Radiolabeled HRV-14 oriI was mixed with various concentrations of unlabeled HRV-14 oriI or PV-1 oriI and incubated with 0.3 μM HRV-14 3C L94P for 15 min at 30°C. Quantification of the protein-RNA complexes on the polysulfone and nitrocellulose membranes shows that mutant HRV-14 3C L94P can rescue the binding between PV oriI and protein. The solid lines represent the fit of the data to a hyperbolic equation with an 50% inhibitory concentration of 0.01 ± 0.001 μM for HRV-14 oriI and 0.16 ± 0.01 μM for PV-1 oriI.

stable as the observed processivity was increased (panel ii of Fig. 6C and D).

Evidence for a two-step mechanism for oriI binding to 3C. The data presented thus far are consistent with the 3C adaptive mutation increasing the affinity of this derivative for PV-1 oriI relative to WT 3C. This possibility was tested by using an RNA filter binding assay (Fig. 7). Previous studies predict the two-step binding mechanism for oriI binding to 3C shown in Fig. 7A (21). oriI binds to two molecules of 3C, facilitating formation of a 3C dimer ($3C_2$), producing a ground-state complex ($3C_2$-oriI) that isomerizes into an activated complex ($3C_2$-oriI*) competent for recruitment of polymerase and uridylylation. We assumed that the $3C_2$-oriI complex would be in rapid equilibrium relative to formation of the $3C_2$-oriI* complex and that formation of the $3C_2$-oriI* complex would be slow and perhaps rate limiting. If this is the case, then the specificity for different oriI elements would likely be manifested in the stability of the $3C_2$-oriI* complex rather than that of the $3C_2$-oriI complex.

We performed a direct binding experiment in which labeled HRV-14 oriI or PV-1 oriI was mixed with different concentrations of 3C for a short period of time (~15 s) to limit the amount of isomerization that could occur followed by filter binding and filter washing steps. The result of this experiment is shown in Fig. 7B. The $K_{0.5}$ value for HRV-14 oriI binding to WT 3C was 30 ± 10 nM; the $K_{0.5}$ value for PV-1 oriI binding to WT 3C was 80 ± 40 nM. These two values are identical within the error of the measurement.

If an isomerized complex exists, then by incubating the binding mixture for longer periods of time, lower $K_{0.5}$ values should be observed in a direct binding mode. The problem is that in order to obtain a $K_{0.5}$ value the concentration of labeled RNA employed must be on the order of 10-fold lower than the $K_{0.5}$ value, causing a substantial reduction in the signal/noise ratio. In order to circumvent this problem, we used a competitive binding mode.

WT 3C was mixed with labeled HRV-14 oriI in the absence or presence of different concentrations of unlabeled competitor (either HRV-14 or PV-1). The binding reaction mixture was incubated for 15 min to permit the reaction to reach equilibrium followed by filter binding and filter washing. If an isomerization step exists that contributes to the specificity of 3C binding, then unlabeled PV-1 oriI should not compete away labeled HRV-14 oriI as well as unlabeled HRV-14 oriI. As shown in Fig. 7C, at equilibrium HRV-14

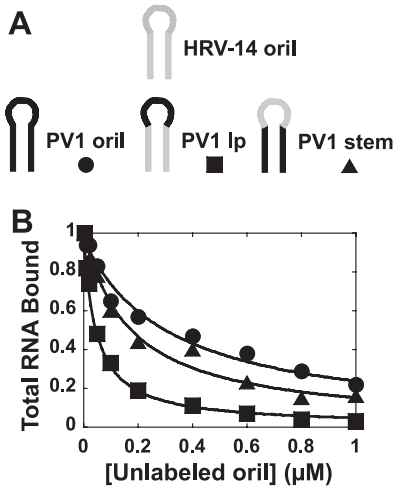

FIG. 8. The primary determinant for 3C binding specificity resides in the oriI stem. (A) Chimeric oriIs used in this study. The loop, stem, or both of HRV-14 oriI were replaced by either the corresponding loop or the corresponding stem of PV-1 oriI. (B) Radiolabeled HRV-14 oriI was mixed with various concentrations of the indicated unlabeled oriIs (PV-1 oriI or PV-1 lp or PV-1 stem) and incubated with 0.3 μM HRV-14 3C WT for 15 min at 30°C. A slot blot apparatus was used in this experiment as described in Materials and Methods. The polysulfone and nitrocellulose membranes bind protein-RNA complex and free protein, and the nylon membrane binds all of the free RNA. ●, unlabeled PV-1 oriI; ■, unlabeled PV-1 lp; ▲, unlabeled PV-3 stem. Quantification of the protein-RNA complexes on the polysulfone and nitrocellulose membranes shows binding competence between HRV-14 oriI and unlabeled oriI (PV-1 oriI or PV-1 lp or PV-1 stem) to HRV-14 3C. The solid lines represent the fit of the data to a hyperbolic equation with a 50% inhibitory concentration of 0.31 ± 0.03 μM for PV-1 oriI, 0.04 ± 0.004 μM for PV-1 lp, and 0.17 ± 0.02 μM for PV-1 stem.

oriI binds to WT 3C 25-fold better than PV-1 oriI. Together, these data provide additional support for the existence of an isomerization step after oriI binding to 3C that imparts specificity to 3C binding.

PV-1 oriI binds to 3C-L94P better than to WT 3C. In order to determine whether 3C-L94P exhibited a change in affinity/specificity for PV-1 oriI, we performed a competition binding experiment as described above. The affinity of 3C-L94P for PV-1 oriI increased by threefold relative to WT 3C (Fig. 7D), providing an explanation for the ability of 3C-L94P to support more robust VPg uridylylation by using PV-1 oriI. A twofold increase in the affinity for HRV-14 oriI was also noted (Fig. 7D). Given the high ground-state affinity of WT 3C for HRV-14 oriI, it is possible that the magnitude of the effect of the adaptive mutation on HRV-14 oriI binding could be greater but is at the limit of resolution for the experimental design.

Evidence for a sequence-specific interaction between 3C and the upper stem of oriI. Direct RNA-binding experiments did not show a substantial difference between binding of 3C to HRV-14 oriI and PV-1 oriI, as the $K_{0.5}$ values for both were in the 30 to 80 nM range (Fig. 7B). We thus conclude that differences in oriI secondary structure (Fig. 2A) do not contribute significantly to the observed difference in oriI recognition by 3C. By using a series of HRV-14/PV-1 oriI chimeras (Fig. 8A), we showed that the upper stem of HRV-14 oriI was more important than the loop in supporting formation of a stable $3C_2$-oriI complex (Fig. 8B), suggesting a sequence-specific interaction between 3C and oriI after unwinding. The preferences observed here were also observed in the context of HRV-14 replicon RNAs containing these chimeric RNAs (32).

DISCUSSION

oriI-dependent VPg uridylylation is essential for production of progeny picornaviral genomes (23). oriI is often described as a bipartite element containing a loop that has sequence (23) and perhaps structural (23) signatures essential for templating VPg uridylylation and a stem that serves only a structural role (23). Numerous observations are consistent with this model. Replication of picornaviruses appears to be much more sensitive to substitutions in the loop than in the stem. Indeed, completely artificial stems have been shown to function for PV-3 (10). PV-1 replication is supported by heterologous oriI elements, for example, that from HRV-14 (25). Therefore, it was quite surprising that PV-3 oriI did not support HRV-14 replication (32). This observation was not related to sequence differences between PV-3 and PV-1 oriI elements (Fig. 2A), as PV-1 oriI did not support HRV-14 replication (Fig. 2C). Interestingly, the inability of HRV-14 to use PV-3 oriI was determined by the stem. An HRV-14/PV-3 chimera containing the PV-3 loop and HRV-14 stem replicated well, suggesting that the stem sequence is an important determinant for oriI function (32). HRV-14 could adapt to use PV-3 oriI by acquiring mutations that changed 3C (L94P) or 3D (D406N) (32). These same changes permitted HRV-14 to use PV-1 oriI (Fig. 2C). The motivation for this study was elucidation of the mechanistic basis for the adaptive changes in HRV-14 3C and 3D with the hope of gaining a better understanding of the structure, function, and mechanism of the PV VPg uridylylation complex.

We established an in vitro VPg uridylylation system for HRV-14 (Fig. 3) that recapitulates the observations made biologically (Fig. 4). The 3D mutation functions at the level of 3Dpol (Fig. 4A). The 3C mutation functions at the level of 3C(D) (Fig. 4B). The two mutations were additive (Fig. 4C), suggesting that each change conferred an independent, new function on the VPg uridylylation complex.

Although the factor and element requirements for VPg uridylylation are well established, the mechanisms for assembly and stability, stoichiometry, and organization of the VPg uridylylation complex have only recently begun to be defined (Fig. 1) (21). Pathak et al. (21) have suggested that a dimer of 3C(D) binds to oriI followed by isomerization of this complex such that the upper stem is unwound. Binding to the upper stem is directed by 3C. The isomerized complex would be stabilized by interaction of 3C molecules with single strands of the upper stem, extending the loop into a conformation more easily bound by 3Dpol. Stable association of 3Dpol with this complex would be mediated by an interaction between the back of the thumb of 3Dpol and surfaces of the 3C dimer. As discussed below, our biochemical analysis of the HRV-14 3C and 3Dpol derivatives that permit use of PV-1 oriI (Fig. 5 to 8) provides additional support for this model.

Although 3C did not exhibit a preference for HRV-14 oriI relative to PV-1 oriI in direct binding experiments (Fig. 7B),

3C exhibited a higher affinity for HRV-14 oriI than PV-1 oriI in competition experiments (compare panel i of Fig. 6A and B to panel i of Fig. 6C and D and Fig. 7C and D). This higher affinity was due to the upper stem, as a PV-1/HRV-14 oriI chimera containing the HRV-14 stem bound to 3C better than a chimera containing the HRV-14 loop (Fig. 8). We conclude that 3C binds to the upper stem of oriI in a sequence-independent fashion that may be structure sensitive. This complex isomerizes into a form that is stabilized by sequence-specific interactions with the upper stem of oriI. A sequence-specific interaction between 3C and the stem would likely require opening after 3C binding, consistent with a two-step binding mechanism (21). Although the bases of double-stranded DNA are accessible from the major groove (20), the bases of double-stranded RNA are much less accessible to protein (5). We propose that HRV-14 3C exhibits greater sequence specificity than PV 3C. The more stringent selection imposed by HRV-14 may be a reflection of the weak binding to oriI suggested by titration experiments: we found a $K_{0.5}$ value of 20 μM for HRV-14 oriI (panel i of Fig. 6A) and a $K_{0.5}$ value of 100 μM for PV-1 oriI (panel i of Fig. 6C). Comparable experiments with PV-1 3C showed a $K_{0.5}$ value of 2 μM for PV-1 oriI (21). If the higher affinity of PV-1 3C for oriI RNAs extrapolates to a broader specificity, then PV-1 would be expected to be less stringent in its selection of oriI elements for replication as reported previously (21).

HRV-14 3C-L94P exhibited a higher affinity than WT 3C for both HRV-14 oriI ($K_{0.5}$ of 10 μM) and PV-1 oriI ($K_{0.5}$ of 20 μM) (panel i of Fig. 6A and C), consistent with the enhanced capacity of the HRV-14 3C-L94P replicon to replicate by using PV-3 (32) or PV-1 oriI (Fig. 2C). HRV-14 3C-L94P still exhibited a preference for binding HRV-14 oriI (Fig. 8). Leu-94 is not conserved across all PV 3C proteins; however, this region of 3C protein has been shown previously to be involved in RNA binding (19). Nayak et al. have shown that residues 92, 95, and 97 of foot-and-mouth disease virus 3C protein are required for foot-and-mouth disease virus oriI binding, VPg uridylylation in vitro, and genome replication in tissue culture (19). We have also identified this region as a determinant for PV-1 oriI binding by PV-1 3C by using nuclear magnetic resonance spectroscopy (unpublished observations). We conclude that after formation of the initial $3C_2$-oriI complex, the duplex opens and each 3C molecule interacts with single-stranded RNA in a sequence-dependent fashion by using residues in the vicinity of residue 94. The adaptive change in 3C not only increases the affinity of this 3C derivative for RNA in general but also expands the sequence specificity of the protein, resulting in the formation of more stable VPg uridylylation complexes. This two-step, sequence-specific binding mechanism observed for 3C binding to oriI may also be required for 3C binding to *cis*-acting replication elements at the 5′ and 3′ ends of picornaviral genomes.

HRV-14 3Dpol-D406N supported increased VPg uridylylation by using either HRV-14 oriI or PV-1 oriI. This substitution also increased the VPg uridylylation activity of PV-1 3Dpol (Table 2). 3Dpol-D406N was not more active than WT 3Dpol, as RNA-primed elongation activity was unchanged (data not shown; also Table 2). HRV-14 3Dpol-D406N assembled more readily into the HRV-14 $3C_2$-oriI complex, as the $K_{0.5}$ value for oriI was reduced by eightfold relative to that of WT 3Dpol to 2 μM (panel i of Fig. 5A). A fivefold reduction in $K_{0.5}$ value to 20 μM was observed when PV-1 oriI was employed (compare panel i of Fig. 6C to panel i of Fig. 6D). HRV-14 3Dpol-D406N was also retained more efficiently in the VPg uridylylation complex because increased processivity was observed relative to WT 3Dpol when VPg (panel ii of Fig. 5C) or PV-1 oriI (panel ii of Fig. 6D) was titrated. Because Asp-406 is located at the top of the thumb of 3Dpol and the back of the thumb has been clearly implicated in an interaction with the 3C dimer for assembly of the VPg uridylylation complex (Fig. 1) (21), we conclude that 3Dpol-D406N assembles more efficiently and more stably with the 3C dimer, leading to increased production of more processive VPg uridylylation complexes.

Assembly of stable VPg uridylylation complexes is essential for picornavirus genome replication. This study suggests that the kinetics of assembly and overall stability of the HRV-14 VPg uridylylation complex exist at the optimal value, leading to a rate of VPg uridylylation that prevents this step in viral RNA synthesis from being rate limiting in infected cells. Substitution of PV oriI into the HRV-14 genome reduces replication, most likely due to a reduced level of VPg-pUpU production (Fig. 3). Although both gain-of-function mutants supported five- to eightfold-increased production of VPg-pUpU (Fig. 4A and B), neither mutant altered the kinetics of HRV-14 genome replication in tissue culture (32). The finding that PV-1 could use HRV-14 oriI without any significant impact on the kinetics of genome replication may suggest that the kinetics of assembly and/or overall stability of the PV-1 VPg uridylylation complex greatly exceed the optimal value. If this is the case, then PV-1 may be more tolerant to changes or disruptions in VPg uridylylation components. For example, it has been suggested that oriI-templated production of VPg-pUpU is not required for PV-1 negative-strand RNA synthesis based on the observation that mutations in PV-1 oriI that severely impair VPg uridylylation have no impact on negative-strand RNA synthesis in a cell-free system (17, 18). If PV-1 produces far more VPg-pUpU than needed, then even a substantial reduction in the concentration of VPg-pUpU may be tolerated. Therefore, it remains possible that oriI is used for negative-strand RNA synthesis (16). Given the sensitivity of HRV-14 to changes in oriI, this system may be useful in clarifying this issue.

ACKNOWLEDGMENTS

This work was supported in part by grants AI053531 (C.E.C.) and AI142082 (S.M.L.) from NIAID/NIH. Y.Y. was supported by a J. W. McLaughlen Postdoctoral Fellowship.

REFERENCES

1. **Ambros, V., and D. Baltimore.** 1978. Protein is linked to the 5′ end of poliovirus RNA by a phosphodiester linkage to tyrosine. J. Biol. Chem. **253:**5263–5266.
2. **Arnold, J. J., and C. E. Cameron.** 2000. Poliovirus RNA-dependent RNA polymerase (3D(pol)). Assembly of stable, elongation-competent complexes by using a symmetrical primer-template substrate (sym/sub). J. Biol. Chem. **275:**5329–5336.
3. **Arnold, J. J., and C. E. Cameron.** 2004. Poliovirus RNA-dependent RNA polymerase (3Dpol): pre-steady-state kinetic analysis of ribonucleotide incorporation in the presence of Mg^{2+}. Biochemistry **43:**5126–5137.
4. **Arnold, J. J., D. W. Gohara, and C. E. Cameron.** 2004. Poliovirus RNA-dependent RNA polymerase (3Dpol): pre-steady-state kinetic analysis of ribonucleotide incorporation in the presence of Mn^{2+}. Biochemistry **43:** 5138–5148.
5. **Draper, D. E.** 1995. Protein-RNA recognition. Annu. Rev. Biochem. **64:**593–620.

6. **Ferrer-Orta, C., A. Arias, R. Agudo, R. Perez-Luque, C. Escarmis, E. Domingo, and N. Verdaguer.** 2006. The structure of a protein primer-polymerase complex in the initiation of genome replication. EMBO J. **25:**880–888.
7. **Gerber, K., E. Wimmer, and A. V. Paul.** 2001. Biochemical and genetic studies of the initiation of human rhinovirus 2 RNA replication: identification of a *cis*-replicating element in the coding sequence of $2A^{pro}$. J. Virol. **75:**10979–10990.
8. **Gohara, D. W., C. S. Ha, S. Kumar, B. Ghosh, J. J. Arnold, T. J. Wisniewski, and C. E. Cameron.** 1999. Production of "authentic" poliovirus RNA-dependent RNA polymerase (3D(pol)) by ubiquitin-protease-mediated cleavage in Escherichia coli. Protein Expr. Purif. **17:**128–138.
9. **Goodfellow, I., Y. Chaudhry, A. Richardson, J. Meredith, J. W. Almond, W. Barclay, and D. J. Evans.** 2000. Identification of a *cis*-acting replication element within the poliovirus coding region. J. Virol. **74:**4590–4600.
10. **Goodfellow, I. G., D. Kerrigan, and D. J. Evans.** 2003. Structure and function analysis of the poliovirus cis-acting replication element (CRE). RNA **9:**124–137.
11. **Korneeva, V. S., and C. E. Cameron.** 2007. Structure-function relationships of the viral RNA-dependent RNA polymerase: fidelity, replication speed and initiation mechanism determined by a residue in the ribose-binding pocket. J. Biol. Chem. **282:**16135–16145.
12. **Lobert, P. E., N. Escriou, J. Ruelle, and T. Michiels.** 1999. A coding RNA sequence acts as a replication signal in cardioviruses. Proc. Natl. Acad. Sci. USA **96:**11560–11565.
13. **Love, R. A., K. A. Maegley, X. Yu, R. A. Ferre, L. K. Lingardo, W. Diehl, H. E. Parge, P. S. Dragovich, and S. A. Fuhrman.** 2004. The crystal structure of the RNA-dependent RNA polymerase from human rhinovirus: a dual function target for common cold antiviral therapy. Structure **12:**1533–1544.
14. **Lyons, T., K. E. Murray, A. W. Roberts, and D. J. Barton.** 2001. Poliovirus 5′-terminal cloverleaf RNA is required in *cis* for VPg uridylylation and the initiation of negative-strand RNA synthesis. J. Virol. **75:**10696–10708.
15. **McKnight, K. L., and S. M. Lemon.** 1996. Capsid coding sequence is required for efficient replication of human rhinovirus 14 RNA. J. Virol. **70:**1941–1952.
16. **McKnight, K. L., and S. M. Lemon.** 1998. The rhinovirus type 14 genome contains an internally located RNA structure that is required for viral replication. RNA **4:**1569–1584.
17. **Morasco, B. J., N. Sharma, J. Parilla, and J. B. Flanegan.** 2003. Poliovirus *cre*(2C)-dependent synthesis of VPgpUpU is required for positive- but not negative-strand RNA synthesis. J. Virol. **77:**5136–5144.
18. **Murray, K. E., and D. J. Barton.** 2003. Poliovirus CRE-dependent VPg uridylylation is required for positive-strand RNA synthesis but not for negative-strand RNA synthesis. J. Virol. **77:**4739–4750.
19. **Nayak, A., I. G. Goodfellow, K. E. Woolaway, J. Birtley, S. Curry, and G. J. Belsham.** 2006. Role of RNA structure and RNA binding activity of foot-and-mouth disease virus 3C protein in VPg uridylylation and virus replication. J. Virol. **80:**9865–9875.
20. **Pabo, C. O., and R. T. Sauer.** 1984. Protein-DNA recognition. Annu. Rev. Biochem. **53:**293–321.
21. **Pathak, H. B., J. J. Arnold, P. N. Wiegand, M. R. Hargittai, and C. E. Cameron.** 2007. Picornavirus genome replication: assembly and organization of the VPg uridylylation ribonucleoprotein (initiation) complex. J. Biol. Chem. **282:**16202–16213.
22. **Pathak, H. B., S. K. Ghosh, A. W. Roberts, S. D. Sharma, J. D. Yoder, J. J. Arnold, D. W. Gohara, D. J. Barton, A. V. Paul, and C. E. Cameron.** 2002. Structure-function relationships of the RNA-dependent RNA polymerase from poliovirus (3Dpol). A surface of the primary oligomerization domain functions in capsid precursor processing and VPg uridylylation. J. Biol. Chem. **277:**31551–31562.
23. **Paul, A. V.** 2002. Possible unifying mechanism of picornavirus genome replication, p. 227–246. *In* B. L. Semler and E. Wimmer (ed.), Molecular biology of picornaviruses, vol. 1. ASM Press, Washington, DC.
24. **Paul, A. V., J. Peters, J. Mugavero, J. Yin, J. H. van Boom, and E. Wimmer.** 2003. Biochemical and genetic studies of the VPg uridylylation reaction catalyzed by the RNA polymerase of poliovirus. J. Virol. **77:**891–904.
25. **Paul, A. V., E. Rieder, D. W. Kim, J. H. van Boom, and E. Wimmer.** 2000. Identification of an RNA hairpin in poliovirus RNA that serves as the primary template in the in vitro uridylylation of VPg. J. Virol. **74:**10359–10370.
26. **Paul, A. V., J. Yin, J. Mugavero, E. Rieder, Y. Liu, and E. Wimmer.** 2003. A "slide-back" mechanism for the initiation of protein-primed RNA synthesis by the RNA polymerase of poliovirus. J. Biol. Chem. **278:**43951–43960.
27. **Rieder, E., A. V. Paul, D. W. Kim, J. H. van Boom, and E. Wimmer.** 2000. Genetic and biochemical studies of poliovirus *cis*-acting replication element *cre* in relation to VPg uridylylation. J. Virol. **74:**10371–10380.
28. **Rothberg, P. G., T. J. Harris, A. Nomoto, and E. Wimmer.** 1978. O4-(5′-uridylyl)tyrosine is the bond between the genome-linked protein and the RNA of poliovirus. Proc. Natl. Acad. Sci. USA **75:**4868–4872.
29. **Thiviyanathan, V., Y. Yang, K. Kaluarachchi, R. Rijnbrand, D. G. Gorenstein, and S. M. Lemon.** 2004. High-resolution structure of a picornaviral internal cis-acting RNA replication element (cre). Proc. Natl. Acad. Sci. USA **101:**12688–12693.
30. **van Ooij, M. J., D. A. Vogt, A. Paul, C. Castro, J. Kuijpers, F. J. van Kuppeveld, C. E. Cameron, E. Wimmer, R. Andino, and W. J. Melchers.** 2006. Structural and functional characterization of the coxsackievirus B3 CRE(2C): role of CRE(2C) in negative- and positive-strand RNA synthesis. J. Gen. Virol. **87:**103–113.
31. **Yang, Y., R. Rijnbrand, K. L. McKnight, E. Wimmer, A. Paul, A. Martin, and S. M. Lemon.** 2002. Sequence requirements for viral RNA replication and VPg uridylylation directed by the internal *cis*-acting replication element (*cre*) of human rhinovirus type 14. J. Virol. **76:**7485–7494.
32. **Yang, Y., R. Rijnbrand, S. Watowich, and S. M. Lemon.** 2004. Genetic evidence for an interaction between a picornaviral cis-acting RNA replication element and 3CD protein. J. Biol. Chem. **279:**12659–12667.
33. **Yin, J., A. V. Paul, E. Wimmer, and E. Rieder.** 2003. Functional dissection of a poliovirus *cis*-acting replication element [PV-*cre*(2C)]: analysis of single- and dual-*cre* viral genomes and proteins that bind specifically to PV-*cre* RNA. J. Virol. **77:**5152–5166.